PRAMANA — journal of physics

Vol. 80, No. 6
June 2013
pp. 971–981

Three-dimensional simulation studies of 10 MeV, 352.2 MHz drift tube Linac

NITA S KULKARNI
Accelerator & Beam Physics Laboratory, Materials and Advanced Accelerator Sciences Division, Raja Ramanna Centre for Advanced Technology, Indore 452 013, India
E-mail: nita@rrcat.gov.in

MS received 30 October 2012; revised 31 January 2013; accepted 18 February 2013

Abstract. It is proposed to build a drift tube Linac (DTL) at Raja Ramanna Centre for Advanced Technology, Indore, India, that will form a part of the future Spallation Neutron Source. This DTL will accelerate 30 mA H-ion beam from 3 MeV to 10 MeV. The DTL is designed to operate at 352.2 MHz with a maximum duty cycle of 3%. The DTL tank will consist of three sections, each about 1.2 m in length having 60 cells. The DTL has a ramped accelerating field, which is ramped in the first section of DTL from 1.8 to 2.2 MV/m and remains constant over the rest of the length of DTL. The field in DTL will be stabilized using post-couplers. The three-dimensional (3D) design of the DTL is done using CST microwave studio (CST MWS) incorporating the various non-axisymmetric components such as tuners, post-couplers and vacuum ports. The frequency shifts due to these components have been evaluated. This paper presents the details of the studies and analysis of 3D simulations of post-couplers, tuners and vacuum ports.

Keywords. Drift tube Linac; electromagnetic simulations; resonant coupling; field stabilization.

PACS Nos 29.20.Ej; 28.52.Av

1. Introduction

A 10 MeV, 352.2 MHz DTL is being built as a part of the front-end injector of the proposed future Indian Spallation Neutron Source. The front-end injector consists of a 50 keV ion source, low energy beam transport (LEBT), 3 MeV radio frequency quadrupole (RFQ) and a 10 MeV drift tube Linac (DTL). Figure 1 shows the schematic of the front end of the injector.

H^- beam at 50 keV from the ion source will be injected into the RFQ, which will be accelerated to 3 MeV in the four-vane RFQ. The DTL would further accelerate the 30 mA beam from 3 MeV to 10 MeV. DTL is an Alvarez kind of structure operating at 352.2 MHz and uses post-couplers for field stabilization. Quadrupoles in FOFODODO lattice were used for transverse focussing. The optimization of the geometrical parameters [1] of the drift tube Linac was done by varying the gap to cell length (g/L) ratio using SUPERFISH

DOI: 10.1007/s12043-013-0542-3; ***e*Publication: 28 May 2013**

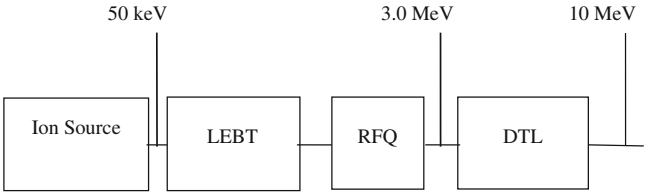

Figure 1. Lay-out of the Linac front end.

[2] to give 10 MeV energy. Figure 2 shows 1/4th of the unit cell geometry. After optimization, a combination of tank diameter (TD) of 52 cm, drift tube diameter (DTD) of 14 cm and bore radii (BR) of 1.0 cm were arrived at as a suitable choice. The post-coupler diameter and stem diameter were taken to be the same to ease fabrication and was selected to be 2.6 cm. The total power loss with 1.25% duty cycle is 9.5 kW, wherein the cavity loss is 6.5 kW. Beam dynamics simulation and cell length computations [3,4] were done using PARMILA [5]. The length of the Linac was 5.62 m with 60 cells. Transmission efficiency of 100% was obtained without much increase in output emittances. For an input beam with a normalized rms emittance of 0.022 cm mrad, the output transverse normalized rms emittance was 0.023 cm mrad and the longitudinal emittance was 0.118 deg MeV.

Two-dimensional (2D) simulations performed with SUPERFISH code allow for a good estimation of power dissipation on the entire cell, i.e., on the stems and post-couplers. However, SUPERFISH cannot analyse the coupling between the post-couplers and drift tube cells resulting in a discrepancy in the frequency. Also the effect on resonant frequency of DTL due to the non-axisymmetric objects like tuners etc. cannot be analysed using a 2D code. Hence 3D simulations are needed to study the coupled cavity fields and the associated mode frequency. The 3D design of the DTL was done using CST

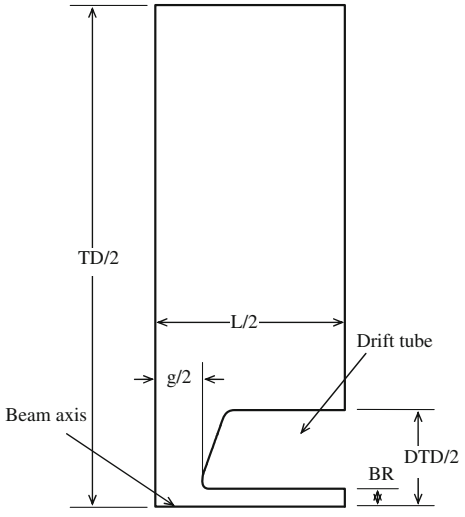

Figure 2. 1/4th unit cell drift tube geometry.

MWS. The effect on resonant frequency of the DTL, due to tuners, vacuum ports and post-couplers was studied. A study on field stabilization using post-couplers was also done.

2. Electromagnetic design and frequency analysis

Components like tuners, post-couplers and vacuum ports break the azimuthal symmetry of the structure. These non-axisymmetric components were modelled in CST MWS and their effect on frequency and field were studied. The MWS eigenmode solver solves for the electric field and frequency, and is highly dependent on mesh size. To overcome the problem of a huge number of mesh points, a few middle cells were modelled and the effect on frequency and field due to tuners, post-couplers and vacuum ports were studied. Figure 3 shows the 3D plots using CST MWS showing tuner, vacuum port and post-couplers.

2.1 *Tuners*

To compensate and adjust the frequency of the DTL, cylindrical rods were provided which when pushed inside perturbed the field leading to the tuning of the cavity. Both bulk (fixed) tuners and slug tuners were used to compensate for the thermal detuning, fabrication errors, beam loading etc. The desired tuning range was estimated to be about 2.5 MHz. One tuner was modelled and the total shift was calculated based on the shift due to one tuner multiplied by the number of tuners. The total tuning range was obtained using a total of 14 equispaced tuners (2 movable and 12 fixed) of 120 mm diameter and 110 mm maximum penetration depth. Analytically, frequency shift due to the tuners can be calculated using Slater's perturbation theorem [6], according to which the frequency shift ($\delta\omega$) is given by

$$\frac{\delta\omega}{\omega} = \frac{\int (\mu H^2 - \varepsilon E^2)\,\mathrm{d}V}{4U}, \tag{1}$$

where H and E are respectively the magnetic and electric fields of the unperturbed cavity mode, μ and ε are the permeability and permittivity respectively and U is the total energy stored in the unperturbed volume. Angular frequency is ω and $\mathrm{d}V$ is the change in cavity volume.

The tuner when penetrates inside, perturbs the magnetic volume of the cavity, thus affecting the inductance and increasing the resonant frequency. On further penetration, both electric and magnetic volumes are affected and hence the rate of increase of frequency reduces. With further penetration, the electric field dominates and frequency starts

Figure 3. CST MWS plots showing tuner, vacuum port and post-couplers.

reducing. Figure 4 shows the effect of tuner penetration for 100 mm and 120 mm diameter tuners on the resonant frequency of DTL. The frequency shift with a tuner of 120 mm diameter and penetration depth of 110 mm using CST MWS was found to be 210 kHz. The frequency shift was also calculated using Slater's perturbation theorem which was found to be 195 kHz. This closely matches with the one obtained using CST MWS. The insertion length of the fixed tuners will be determined during the low power characterization and then these will be machined and fixed, i.e. all tuners are movable for low-power characterization.

2.2 *Vacuum port*

To get the desired vacuum in the DTL tank, it is planned to have a provision of two vacuum ports per section of the DTL. Vacuum port will be slotted in order to have minimum leakage of power and the slots are in the direction of the RF current so that their effect and frequency perturbation are minimized. A vacuum port was simulated with a total of five slots. The frequency shift due to one vacuum port was 13 kHz which was negligible and six ports were located along the entire DTL tank.

2.3 *Post-coupler*

DTL is a cavity operating in TM_{010} mode. The fields in all the cells are in the same phase, i.e. the overall cell array operates in the zero mode which is characterized by zero group velocity. Thus the field in the DTL is very sensitive to perturbations which may arise due to thermal detuning, beam loading and structure imperfections. The field stabilization in accelerators operating in zero mode can be obtained using the resonant coupling approach [7]. Figure 5 shows the drift tube Linac with post-couplers used for stabilization.

Field distribution in an accelerating cavity is a complicated function of wall losses, manufacturing errors and beam loading. Post-couplers (PC) are used in DTL cavities to stabilize the accelerating field in case of local field errors by creating a secondary coupled resonator system which is coupled to the main resonator system formed by the drift tube cells.

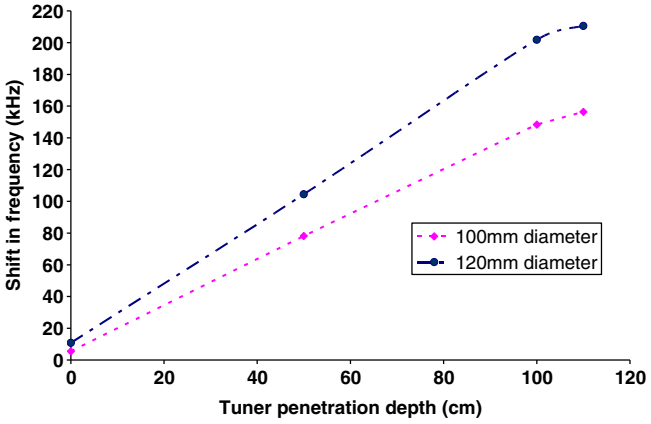

Figure 4. Tuner penetration depth vs. shift in resonant frequency.

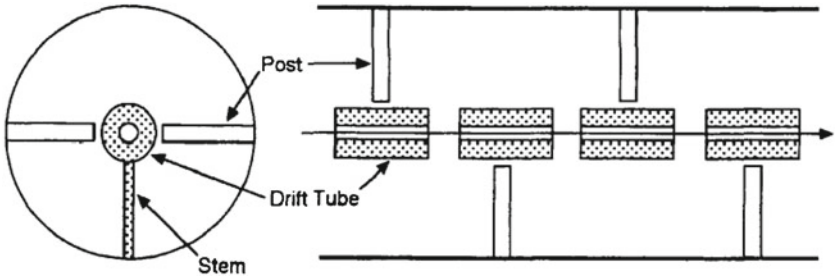

Figure 5. Drift tube Linac with post-couplers for field stabilization.

Basically tuning of the post-coupler has to achieve the following two things simultaneously: (1) Close the stop band between the dispersion curve of the post mode (TE mode) and that of the TM mode [8]; (2) increase the similarity between the field distribution of the TM_{011} and that of TE mode (PC_1) due to post-coupler along the beam axis. Figures 6a and b show the confluence of two pass-bands without coupling between merging pass-bands and with coupling between the two merging pass-bands respectively. As shown in figure 6b the slope of the dispersion curve is linear around the operating point and the frequency difference between modes across the operating mode is equal and opposite, leading to the cancellation of their effect and hence better stability. Figure 7 shows

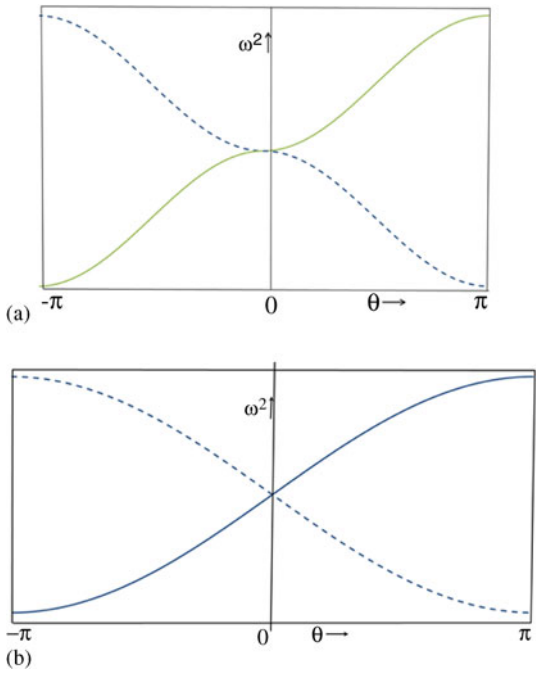

Figure 6. Confluence of two pass-bands (**a**) without coupling and (**b**) with coupling between the two merging pass-bands, i.e. the stabilized case.

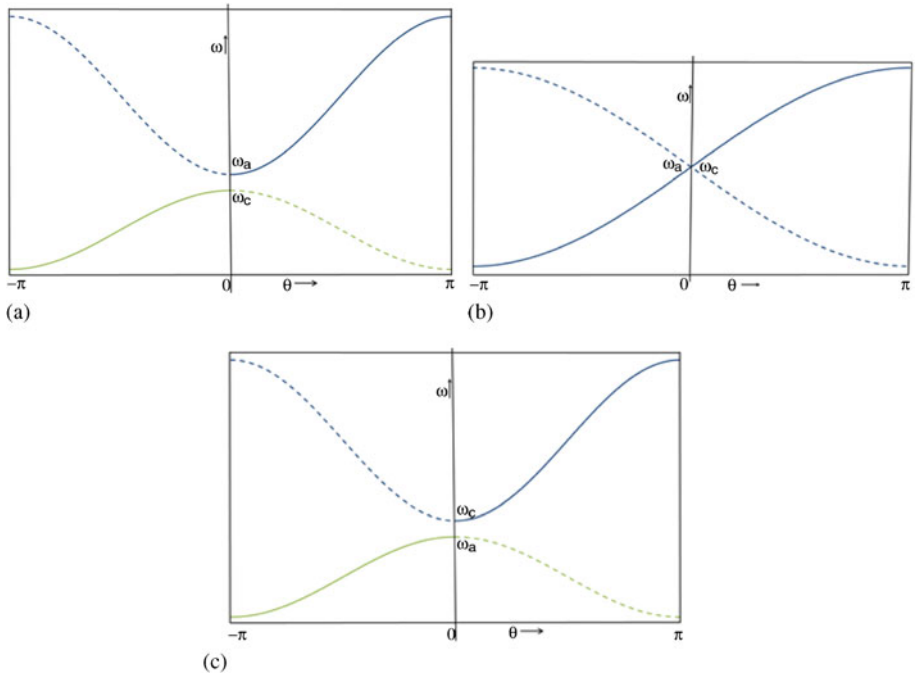

Figure 7. Dispersion curve of a structure with resonant coupling. (**a**) Undercompensated case, (**b**) compensated case and (**c**) overcompensated case.

the dispersion curve of a structure with post-couplers as coupling elements used for resonant coupling. The zero-mode resonant frequency of the accelerating cavity is ω_a and the zero-mode resonant frequency of the coupling element is ω_c. For the undercompensated case $\omega_c < \omega_a$, for the compensated structure $\omega_c = \omega_a$ and for the overcompensated case $\omega_c > \omega_a$. Improved stability is obtained for the compensated case when the frequency of the highest mode of coupling element pass-band coincides with the lowest mode of the accelerating pass-band, leading to two merging pass-bands symmetric about the operating point, i.e. at confluence.

2.3.1 *Mechanism of stabilization.* A post-coupled structure can be represented by an equivalent LC circuit [9]. When post-couplers are inserted in the tank, the capacitance between a post-coupler tip and drift tube and the inductance around a post-coupler makes a resonant circuit. Figure 8 shows the equivalent circuit of a post-coupled structure. Here, L_0 and C_0 represent the inductance of the drift tube and its capacitance to the outer tank wall respectively, C_1 and L_1 represent the capacitance of the gap between the drift tube and inductance of the supporting stem respectively. L_2 and C_2 represent respectively the inductance of the post and its capacitance to the drift tube. M_0, M_1 and M_2 are the mutual inductances.

The equivalent circuit of post-couplers shows that all post-couplers form a chain of oscillators and a new dispersion curve of post-couplers arises. This coupled resonator

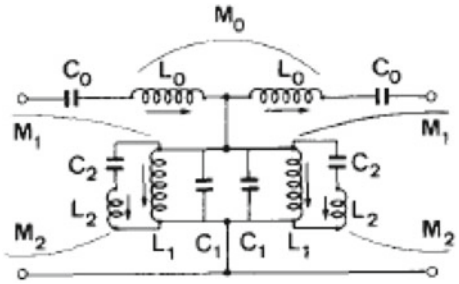

Figure 8. Equivalent circuit of a post-coupled structure.

system has two chains of resonators, two bands of frequencies namely, TM band of the drift tubes and PC band or TE band of the post-couplers. Since posts are located at the symmetry of the structure, it has little effect on TM_{010} mode but has an effect on TM_{01x} modes. The length of the post-couplers is tuned to couple the post-mode with a TM_{01x} kind of accelerating mode. As a result of confluence, the dispersion curve near the operating point has a finite slope, i.e. a non-zero group velocity, and due to this finite group velocity, there is an energy flow and it becomes harder to excite higher-order modes. The stabilization of the field is obtained and at the stabilization point, resonant frequency remains constant for all kinds of perturbations.

2.3.2 *Field analysis with CST MWS.* CST MWS is used to model four cells with three post-couplers alternately located from one side to the other along the horizontal axis from each other. The total number of mesh cells is 27,21,205. Figure 9 shows the drift tube and post-coupler simulated using CST MWS. As shown in the figure, the post-couplers are located alternately at 180° from one drift tube to another. This placement widens the pass-band. Stems are located at 90° to the post-couplers to minimize the coupling between the posts and the stems. Excellent stability is provided by placing the post-couplers adjacent to every other full drift tube and hence each tank has to have even number of cells to facilitate this placement scheme. Generally, less number of post-couplers are preferred as these lead to additional losses resulting in a decrease in Q value. Figure 10 shows the field configuration for both the fundamental TM_{010} mode and the post-coupled mode. Both the nearest neighbouring modes of $TM_{010,}$ i.e., TM_{011} and the post mode PC_1 play important roles in stabilization.

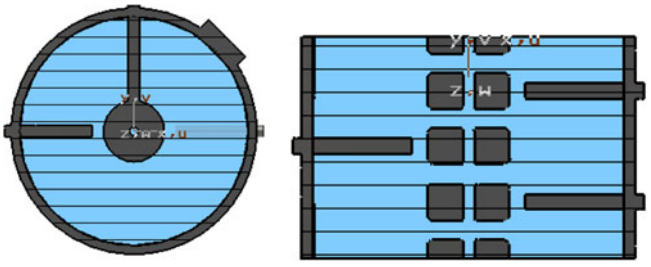

Figure 9. Drift tube tank with drift tube and post-coupler simulated using CST MWS.

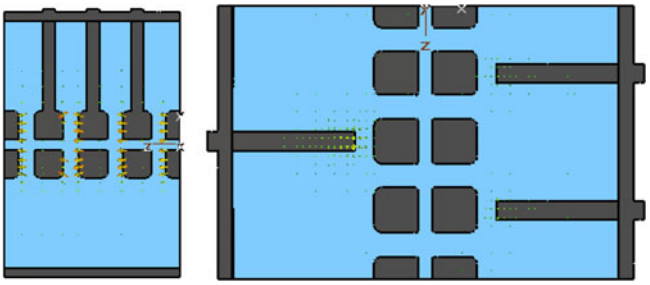

Figure 10. Field configuration for the fundamental mode (TM_{010}) and the lowest order post-coupled mode (TE) using CST MWS.

Each post-coupler has a tab on the top of the bar and will have 360° rotational adjustment and a full tank penetration adjustment. Post-coupler tabs will be used to attain the desired field distribution [9]. Figure 11 shows the post-coupler with tabs generated using CST MWS. The tip of the post-coupler should not come in contact with the drift tubes. Each post-coupler requires a unique length and a rotational orientation. The tilt of each tab will be fixed after adjusting the insertion length of the post-coupler. Initially, every post-coupler will be inserted uniformly during the cold test and then the tilt of each tab will be adjusted one by one.

Post-couplers of different diameters ranging from 2 to 2.6 cm were modelled and studied for the point of confluence. Figure 12 shows the effect on the post-mode frequency with different radii and lengths of the post-couplers. Post-coupler diameter was selected the same as stem diameter, i.e. 2.6 cm, to ease material procurement and for fabrication simplicity. When the diameter of post-coupler is 2.6 cm, the length to attain confluence is 16.62 cm. It is concluded from simulations that as the radii of the post-coupler decreases, the penetration depth has to be increased to maintain the point of confluence.

The effect of post-coupler insertion length on the fundamental resonant frequency for 1.3 cm post-coupler radius is shown in figure 13. The final depth of penetration with fine tuning and tab rotation will be based on low-power characterization. Figure 14 shows the field ramp obtained with tabs rotated completely towards the right and left with respect to the low energy end of DTL. Post-couplers of 1.3 cm radii at a penetration depth of 16.62 cm lead to confluence and hence to a stabilized or compensated structure.

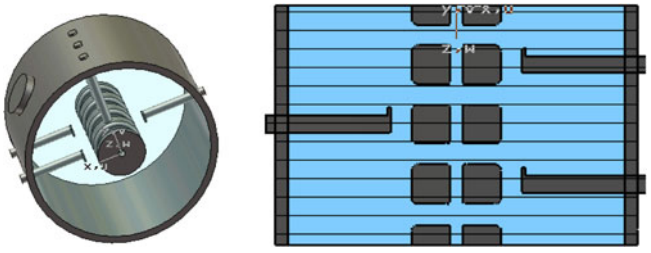

Figure 11. Post-couplers with tab generated using CST MWS.

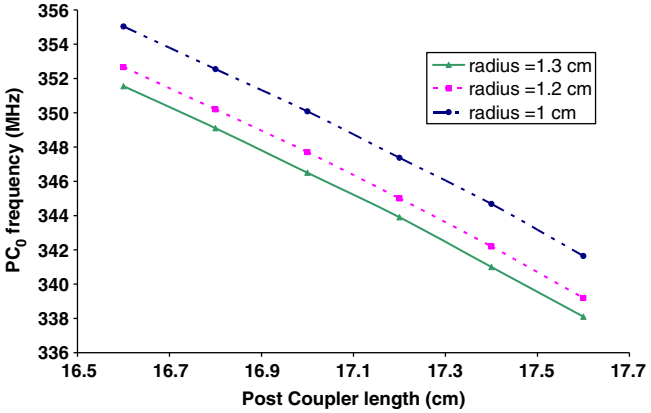

Figure 12. TE mode frequency as a function of post-coupler length and radius.

3. Current status

Based on the physics design presented in this paper, thermal-hydraulic analyses have been performed for the DTL tank and drift tube–stem assembly using ANSYS. The entire length of the DTL tank will be divided into three segments for ease in mechanical fabrication. Initially, the first segment will be fabricated and low-power characterization will be done on this. The temperature, pressure and velocity distribution in the cooling passage were evaluated. Based on the port size specified in this paper, vacuum pump-down calculations were carried out for the DTL and pump capacity has been decided. One independent vacuum system for each tank comprising of a 500 l/s turbo-molecular pump and three 500 l/s sputter ion pumps will be used. A system for mounting and alignment of

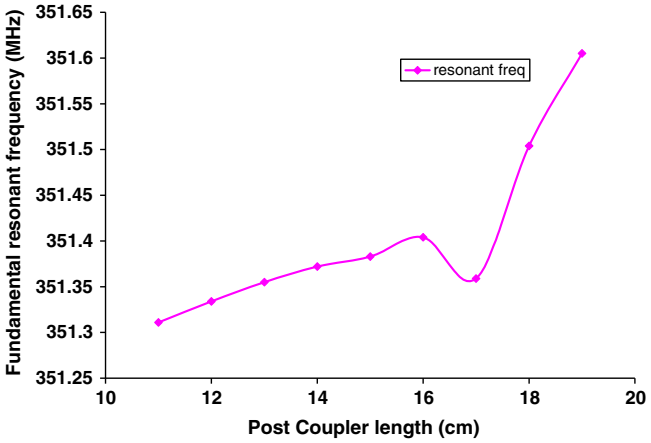

Figure 13. Resonant frequency vs. post-coupler length for a post-coupler radius of 1.3 cm.

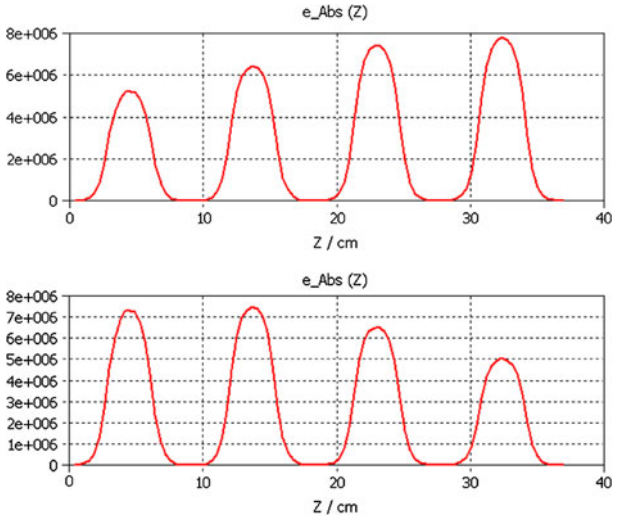

Figure 14. Field ramp with tab direction towards the extreme right and left respectively.

drift tubes has been designed which can align the drift tubes in all six degrees of freedom. Engineering drawings for the DTL structure have been prepared based on the mechanical design analysis and calculations.

4. Conclusion

The 3D design of the DTL is done using CST MWS incorporating various non-axisymmetric components like tuners, post-couplers and vacuum ports. The frequency shifts due to these have been calculated.

The desired tuning range of 2.5 MHz is obtained using a total of 14 equispaced tuners (2 movable and 12 fixed) of 120 mm diameter and with a maximum penetration depth of 110 mm. The frequency shift obtained with 120 mm diameter tuner and 110 mm penetration depth using CST MWS was found to be 210 kHz which closely matches with the one calculated using Slater's perturbation theorem. There is a negligible frequency shift due to the vacuum port and six such ports will be located along the entire DTL tank. The length to attain confluence is 16.62 cm for a 2.6 cm diameter post-coupler. It is concluded from simulations that as the radii of the post-coupler decreases, the penetration depth has to be increased to maintain the point of confluence.

Based on the physics design, engineering design is done for the first segment and fabrication is being taken up. Heat calculations are done using which the cooling channels are designed by taking into account the thermal considerations. In particular, a detailed study on field stabilization using post-couplers was done and the post-coupler length was deduced which will be ascertained using bead pull measurements once the prototype segment of the DTL is obtained from fabrication. The desired field profile will be obtained using tab rotation during low-power characterization.

Acknowledgements

The author is thankful to Dr S B Roy for his continuous support and to Dr Vinit Kumar for going through the manuscript and render useful suggestions. The author also thanks Los Alamos Accelerator Code Group for providing the codes SUPERFISH and PARMILA.

References

[1] Nita S Kulkarni and P Shrivastava, *Proceeding of the Indian Particle Accelerator Conference* (2009)
[2] J H Billen and L M Young, POISSION/SUPERFISH, LA-UR-96-1834 (1996)
[3] N S Kulkarni, P Shrivastava and P Singh, RRCAT Internal Report, RRCAT/2010-05
[4] N S Kulkarni and P Shrivastava and P Singh, RRCAT Internal Report No. RRCAT/2010-08
[5] H Takeda, PARMILA, LA-UR-98-4478, LANL (1998)
[6] J C Slater, *Microwave electronics* (D Van Nostrand, Princeton, NJ, 1950) pp. 80–81
[7] D E Nagle, E A Knapp and B C Knapp, *Rev. Sci. Instrum.* **38(11)**, 1583 (1967)
[8] J Ungrin, S O Schriber and R A Vokes, *IEEE Trans. Nucl. Sci.* **NS-30**, 3013 (1983)
[9] Pierre M Laposttotle and Albert L Septier, *Linear accelerators* (North Holland Publishing Company, Amsterdam, 1970)